Doping-Spike PtSi Schottky Infrared Detectors with Extended Cutoff Wavelengths

T. L. Lin, J. S. Park, S. D. Gunapala, E. W. Jones, and H. M. Del Castillo

Center for Space Microelectronics Technology

Jet Propulsion Laboratory, California Institute of Technology

Pasadena, CA 91109

ABSTRACT

A technique incorporating a p+ doping spike at the silicide/Si interface to reduce the effective Schottky barrier of the silicide infrared detectors and thus extend the cutoff wavelength has been developed. In contrast to previous approaches which relied on the tunneling effect, this approach utilizes a thinner doping spike (< 2 nm) to take advantages of the strong Schottky image force near the silicide/Si interface and thus avoid the tunneling effect. The critical thickness, i. e., the maximum spike thickness without the tunneling effect has been determined and the extended cutoff wavelengths have been observed for the doping-spike PtSi Schottky infrared detectors. Thermionic-emission-limited and thermally-assisted tunneling dark current characteristics were observed for detectors with spikes thinner and thicker than the critical thickness, respectively.

L INTRODUCTION

Silicide Schottky infrared (IR) detectors offer promise of a low-cost, rugged, medium wavelength infrared (MWIR) thermal imaging technology with advantages in silicon-based fabrication, producibility, array size, response uniformity, and low I/f noise [1]. State-of-the-art 640 x 480- and 1024 x 1024-element PtSi focal plane arrays, with cutoff wavelengths ranging from 5.1 to 5.9 pm, are used for imaging in the 3-5 μm medium wavelength infrared (MWIR) region[2-5].

The spectral response of the silicide Schottky IR detector follows the modified Fowler equation, given by

$$\eta = C_1 \frac{(h\nu-\Psi_0)^2}{h\nu} = 1.24\, C_1 \lambda \left(\frac{1}{\lambda} - \frac{1}{\lambda_c}\right)^2 \qquad (1)$$

where η is the quantum efficiency (QE), C_1 is the emission coefficient, hv and λ are the energy and the wavelength of the incident photon, respectively, Ψ_0 is the optical potential barrier, and λ_c is the cutoff wavelength, given by

$$\lambda_c = \frac{1.24}{\Psi_0}. \qquad (2)$$

There is a great interest in extending the PtSi cutoff wavelength for long wavelength infrared (LWIR) operation in the 8-14 μm regime and for improved M WIR performance as given by Eq. 1. Previously, we have demonstrated extended PtSi cutoff wavelengths ranging from 5.7 to 22 μm by incorporating a thin (< 1.1 nm) p^+ doping spike at the PtSi/silicon interface [6,7], As shown in Fig. 1(a), the effective Schottky barrier height is determined by the combined effects of the image-force effect and the electric field of the depletion region, This doping-spike technique takes advantages of the strong Schottky image force within ~2 nm from the PtSi/Si interface, as shown in Fig. 1 (b). The barrier reduction $\Delta\Psi$ due to the introduction p+ doping spike can be given approximately by

$$\Delta\Psi = \frac{q}{2\,\varepsilon_{Si}} N d^2 \qquad (3)$$

where N and d are the doping concentration and the thickness of the doping spike, respectively. There is a maximum doping spike thickness, d_c, for the potential reduction without the tunneling effect. Previous cutoff extension approaches utilized doping spikes significantly thicker the critical thickness d_c, resulting in the formation of potential spikes near the silicide/Si interface, and thus required an additional tunneling process for the collection of photo-excited carriers with drastically reduced detector response [8,9].

In this paper, we demonstrate the extended cutoff wavelengths of the doping-spike PtSi Schottky infrared detectors and determine the critical thickness, d_c. Thermionic-emission-limited and thermally-assisted-tunneling dark current characteristics were observed for PtSi detectors with spike thickness smaller and larger than d_c, respectively.

II. CRITICAL SPIKE THICKNESS

The potential in the Si near the silicide/Si for the doping-spike detector is given by [10]

$$\phi(x) = \left(q\frac{N(2d-x)}{2\varepsilon_{Si}} + E\right)x + \frac{q}{16\pi\varepsilon_{Si}x} \quad \text{for } x < d \quad (5a)$$

$$= \sqrt{\frac{2qN_sV}{\varepsilon_{Si}}}(x-d) - \frac{qN_s(x-d)^2}{2\varepsilon_{Si}} + \frac{q}{16\pi\varepsilon_{Si}x} + \left(\frac{qNd^2}{2\varepsilon_{Si}} + Ed\right) \text{ for } x > d \quad (5.b)$$

$$E(x) = -\frac{d\phi}{dx} = \frac{q}{16\pi\varepsilon_{Si}x^2} - \frac{qN(d-x)}{\varepsilon_{Si}} - E \quad \text{for } x < d \quad (6a)$$

$$\frac{q}{16\pi\varepsilon_{Si}x^2} + \frac{qN_s(x-d)}{\varepsilon_{Si}} - E \quad \text{for } x > d \quad (6.b)$$

where Ns is the doping concentration of the substrate, V is the bias voltage, *E is* the electric field at x = d due to the depleted region, given by $E = \sqrt{2qN_s(V+\phi)/\varepsilon_{Si}}$, and ϕ is the Schottky barrier. As indicated in Eq. 6, E (x) is larger than zero for x near the silicide/Si interface and for $x > d$ due to the strong Schottky effect. However, due to the degenerate doping concentration, N of the doping spikes, for spikes thicker than a critical thickness d_c, E(x) may be less than zero for $x < d$, resulting in the formation of a thin potential spike at $x < d$, facilitating the tunneling effect as

shown in Fig. l(b). Consequently, it is required that E(x) > 0 for x < d to avoid the tunneling effect, i.e.,

$$\frac{q}{16\pi\varepsilon_{Si}x^2} - \frac{qN(d-x)}{\varepsilon_{Si}} - E > 0 \qquad \text{for } x < d. \qquad (7)$$

Therefore, the critical spike thickness, d_c is given by

$$d_c \le \frac{3/4}{\pi^{1/3}N^{1/3}} - \frac{\varepsilon_{Si}E}{qN} \simeq \frac{3/4}{\pi^{1/3}N^{1/3}} \qquad (8)$$

Figure 2 shows the critical thickness for the doping spikes as a function of the spike doping concentration. As the doping concentration increased from 10^{19} to 10^{21} cm^{-3}, the critical spike thicknesses decreases from 2.4 to 0.5 nm. The critical thickness is not sensitive to the bias voltage, especially for higher doping concentration, as is expected from Eq. 8. Also shown in Fig. 2 are two curves for potential reduction of 0.05 and 0.15 eV, respectively, given by Eq. 3. A critical spike thickness of 2.1 nm and a doping concentration of 1.5×10^{19} cm^{-3} are required for the 0.05 eV potential reduction, which corresponds to a cutoff wavelength of 6.5 μm for the PtSi detector. A significantly smaller spike thickness (<0.7 nm) with a doping concentration as high as 4×10^{20} cm^{-3} is required for the 0.15 eV potential reduction (14 μm cutoff). The sharp doping profile required was made possible by the recent advances in the silicon molecular beam epitaxy (MBE) technology[6].

The critical thickness and the corresponding doping concentration for a specific potential reduction can be determined by combining Eq. 3 and Eq. 8, given by

$$d_c = 0.211 \frac{q}{\pi \varepsilon_{Si} \Delta\Psi} \qquad (9)$$

$$N = 44.9 \frac{\pi^2 \varepsilon_{Si}^3 \Delta\Psi^3}{q^3} \qquad (10)$$

Figure 3 shows the critical thickness and the corresponding doping concentration as a function of the potential reduction and the extended cutoff wavelength for PtSi detectors assuing a Schottky barrier height of 0.24 eV. As shown in Fig. 3, thinner doping spikes with higher doping

concentrations are required for larger potential reductions and longer extended cutoff wavelengths.

III. DETECTOR FABRICATION

Five PtSi detectors were fabricated on double-side polished Si (100) wafers with a resistivity of 30 Ω-cm. These doping-spike PtSi detectors incorporated p^+ spikes at the PtSi/Si interface with thicknesses ranging from 0.7 to 1.1 nm and boron doping concentrations ranging from 5 x 10^{19} to 2 x 10^{20} cm^{-3}, and the PtSi layers were 4-rim-thick, The p^+ doping spikes were grown by MBE. The details of the MBE growth of the p^+ doping spikes and the PtSi formation were given elsewhere [6,7]. The device structure incorporated n-type guard rings which defined the periphery of the active device areas to suppress the edge leakage. Neither an anti-reflection coating nor an optical cavity was incorporated in these test devices. The corresponding spike thicknesses and doping concentrations of these detectors were also indicated in Fig. 2.

IV. DETECTOR CHARACTERISTICS AND DISCUSSION

Thermionic-emission limited current characteristics were observed for all detectors, and the thermal potential barrier Ψ_t and the Richardson constant A** were determined by plotting in (J_o/T^2) versus 1/kT (the activation energy plot) at -0.5V bias, where Jo is the dark current density and T is the absolute temperature. The spectral responses of these detectors were measured with back-side illumination using a blackbody source at 40K and biased at -0.5 V. Figure 4 shows the activation energy plot and the spectral response of a typical LWIR doping-spike PtSi detector (sample E). The cutoff wavelengths and the corresponding optical potential barrier Ψ_o for the detectors were determined by the modified Fowler plot. Thermal potential barriers 'P_t ranging from 0.051 to 0.218 eV and A** ranging from 0.1 to 73 A $cm^{-2}K^{-2}$ were measured form these plots. Optical potential barriers Ψ_o ranging from 0.088 to 0.216 eV, corresponding to cutoff wavelengths ranging from 14 to 5.74 μm were determined from the linear portions of the modified Fowler plots. The spike thickness, the doping concentration, the thermal potential barrier Ψ_t, the Richardson constant A**, the optical potential barrier Ψ_o were shown in Table 1.

As shown in Fig. 2, the thicknesses and the doping concentrations of the spikes of sample D and E were in the tunneling region. We noted that for these two samples $'I'_t$ were dramatically lower than their Ψ_0 ($\Psi_0 - \Psi_t$ of 0.056 and 0.037 eV for sample D and E, respectively, compared to< 0.004 eV for sample A, B, and C) and A** were much smaller than those of other samples. As shown in Fig. 1 (b), the band structure of sample E exhibits a local potential maximum at x = d (0.9 rim), which allows the accumulation of thermally-generated holes and their subsequent tunneling through the potential barrier peaked at $x \simeq 5$ nm, resulting in an smaller effective potential barrier $'I'_t$. However, due to the short lifetime of the photo-excited holes, their collection through the tunneling process is very difficult, and therefore, a larger optical barrier Ψ_0 was observed from the photoresponse measurement. The smaller A** observed for sample D and E possibly resulted from the additional tunneling process.

V. SUMMARY

A doping spike technique for the extension of silicide Schottky IR detector cutoff wavelength has been developed and extended cutoff wavelengths have been observed for the doping-spike PtSi Schottky infrared detectors. The critical thickness of the doping spike without the tunneling effect has been determined. Thermionic-emission-limited and thermally-assisted tunneling dark current characteristics were observed for detectors with spikes thinner and thicker than the critical thickness, respectively.

ACKNOWLEDGMENTS

The work described in this report was performed by the Center for Space Microelectronics Technology, Jet Propulsion Laboratory, California Institute of Technology and was jointly sponsored by the National Aeronautics and Space Administration/Office of Advanced Concepts and Technology, the Ballistic Missile Defense Organization/Innovative Science and Technology Office, and the Air Force Rome Laboratory.

REFERENCES

[1] F. D. Shepherd, "Silicide infrared staring sensors," Proc, SPIE, vol. 930, p. 1, 1988.

2] D. J. Sauer, F. V. ShallCross, F. L. Hsueh, G. M. Meray, P. A, Levine, H. R. Gilmartin, 'I'. S, Villani, B. J. Esposito, and J. R. Tower, "640 x 480 MOS PtSi IR sensors," Proc. SPIE, Vol. 1540, *Infrared Technology XVII*, edited by B. F. Andresen, M. Scholl, and I. J. Spiro, pp. 285-296 (SPIE, Bellingham, 1991).

[3] J. L. Gates, W. G, Connelly, T. D. Franklin, R. E, Mills, F. W. Price, and T. Y. Wittwer, "488 x 640-element platinum silicide Schottky focal plane array," Proc. SPIE, Vol. 1540, *Infrared Technology XVII*, edited by B. F. Andresen, M. Scholl, and I. J. Spiro, pp. 297-302, (SPIE, Bellingham, 1991).

[4] D. L. Clark, J. R. Berry, G. L. Compagna, M. A, Cosgrove, G. G. Furman, J. R, Heydweiller, H. Honickman, R. A. Rehberg, P. H. Solie, and E. T. Nelson, "Design and performance of a 486 x 640 pixel platinum silicide IR imaging system," Proc. SPIE, Vol. 1540, *Infrared Technology XVII*, edited by B. F. Andresen, M. Scholl, and I, J. Spiro, pp. 303-311, (SPIE, Bellingham, 1991).

[5] M. Kimata, N. Yutani, and S. N. Tsubouchi, "High performance 1040 x 1040 element PtSi Schottky-barrier image sensor," Proc. SPIE. Vol. 1762, *Infrared Technology XVIII*, edited by B. F. Andresen and F. D. Shepererd (SPIE, Bellingham, 1992)

[6] T. L. Lin, J. S. Park, T. George, E. W. Jones, R. W, Fathauer, and J. Maserjian, "Long-wavelength PtSi infrared detectors fabricated by incorporating a p^+ doping spike grown by molecular beam epitaxy," Appl. Phys. Lett., vol. 62, pp. 3318-3320, 1993,

[7] T. L. Lin, J. S. Park, S. D. Gunapala, E. W."Jones, H. M, Del Castillo, M. M. Weeks and P. W. Pellegrini, "7 μm Cutoff PtSi Schottky Infrared Detector with Low Dark Current Characteristics," submitted to IEEE Electron Devices Letters.

[8] C. Y. Wei, W. Tantraporn, W. Katz, G, Smith, "Reduction in the effective barrier height in ptsi-p-si schottky diodes by using low-energy ion-implantation," Thin Solid Films, 93, pp. 407-412, 1982.

[9] P. Pellegrini, M. Week, and C. E. Ludington, Proc. SPIE, Vol. 311, *Mosaic focal Plane Methodologies II*, edited by W. S. Chan and J. T. Hall, pp. 24-29 (SPIE, Bellingham, 1981).

[10] S. M. Sze, *Physics of Semiconductor Devices* (Wiley, New York, 1981), Chap. 5.

FIGURE CAPTIONS

Figure 1. Calculated energy band diagrams of two doping-spike PtSi detectors within 8 nm form the PtSi/Si interface: (a) with a 0.9-nm-thick spike, [B] = 10^{20} cm^{-3} and (b) with a 0.9-nm-thick spike, [B] = 2.3x 10^{20} cm^{-3}.

Figure 2. Critical thickness for the doping spike versus spike doping concentration. Also shown are two curves for 0.05 and 0.15 eV potential reduction given by Eq. 3. The p^+ spike thicknesses and doping concentrations of the doping-spike PtSi samples are indicated.

Figure 3. Critical thickness and doping concentration of the doping spike as a function of the potential reduction.

Figure 4. Activation energy plot (a) and the spectral response (b) of a typical 14 μm cutoff backside-illuminated doping-spike PtSi detector (sample E). Neither an optical cavity nor an anti-reflection coating was incorporated in this detector.

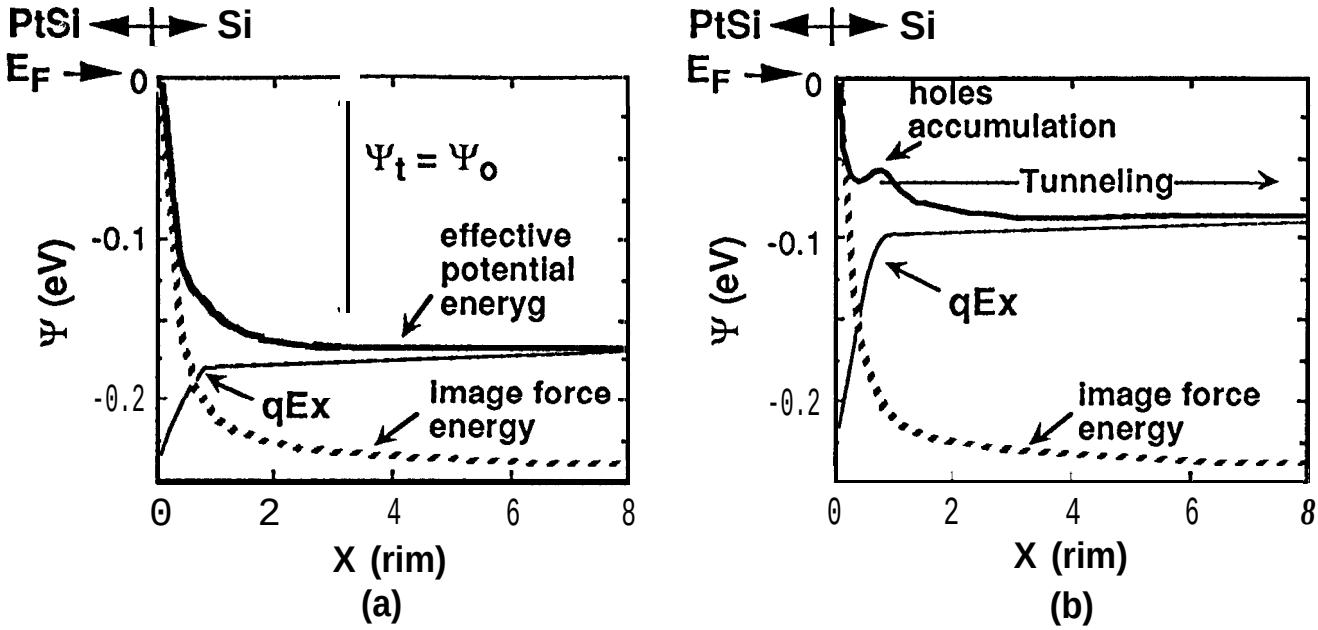

Figure 1. Calculated energy band diagrams of two doping-spike PtSi detectors within 8 nm form the PtSi/Si interface: (a)with a 0.9-nm-thick spike, [B] = 10^{20} cm^{-3} and (b) with a 0.9-nm-thick spike, [B] = 2.3 x 10^{20} cm^{-3}.

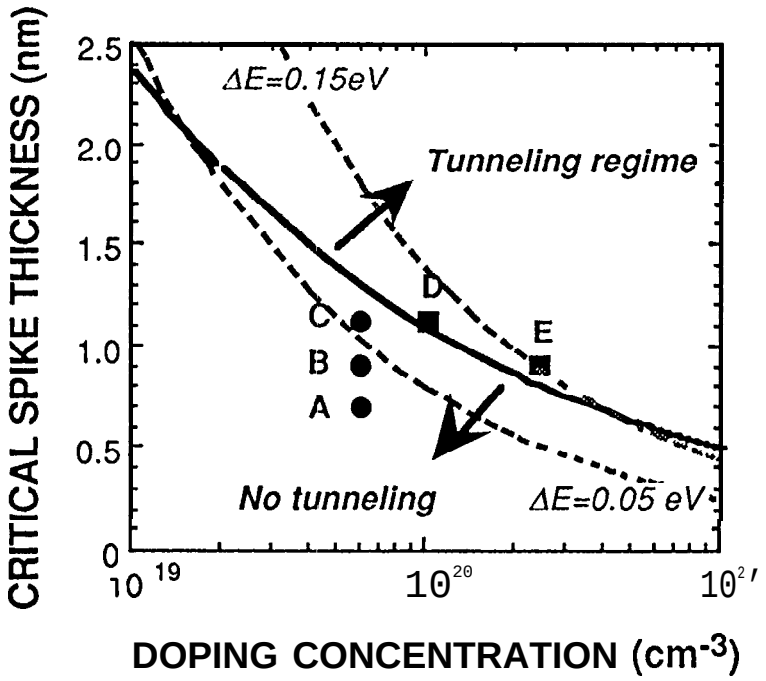

Figure 2. Critical thickness for the doping spike versus spike doping concentration. Also shown are two curves for 0.05 and 0.15 eV potential reduction given by Eq. 3. The p^+ spike thicknesses and doping concentrations of the doping-spike PtSi samples are indicated,

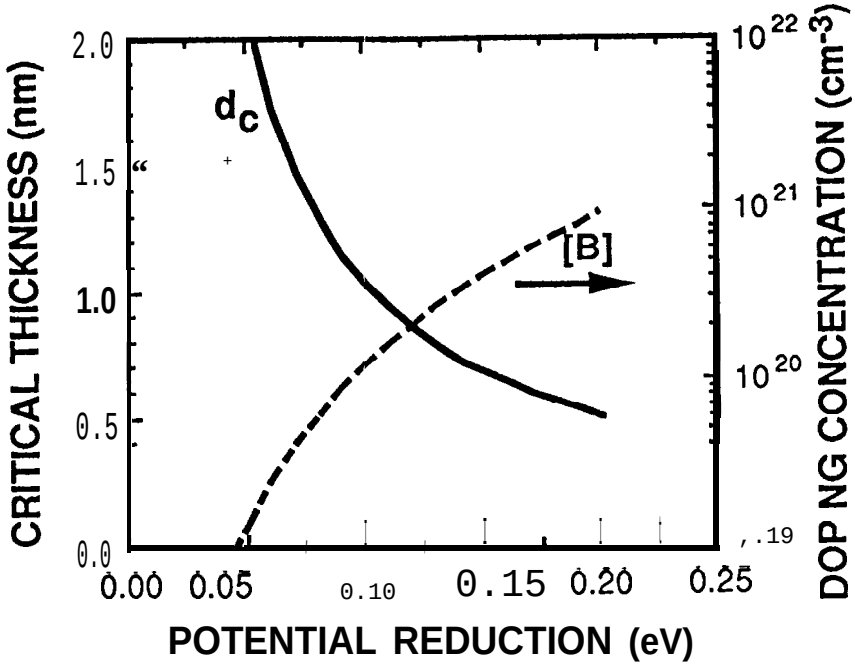

Figure 3. Critical thickness and doping concentration of the doping spike as a function of the potential reduction.

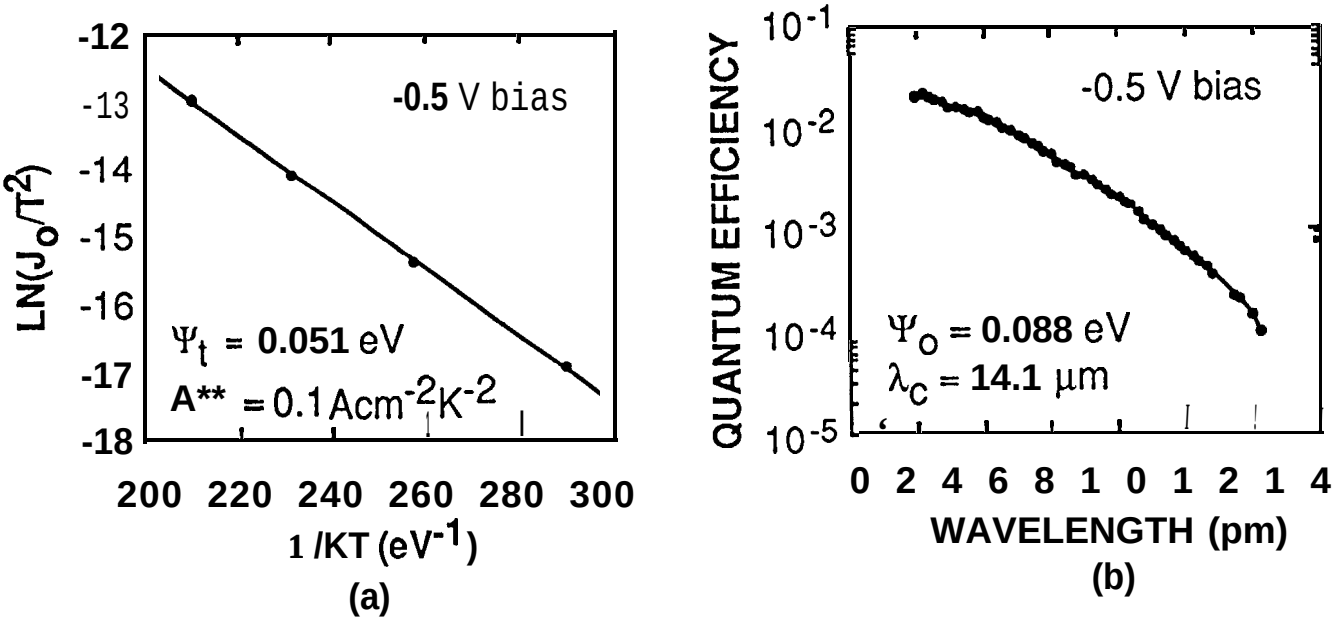

Figure 4. Activation energy plot(a) and the spectral response (b) of a typical 14 μm cutoff backside-illuminated doping-spike PtSidetector (sample E). Neither an optical cavity nor an anti-reflection coating was incorporated in this detector,

TABLE 1. The spike thickness d, the spike doping concentration [B], the thermal potential barrier Ψ_t, the Richardson constant A**, the optical potential barrier Ψ_o, and the cutoff wavelength λ_c for the doping-spike PtSi detectors.

Sample #	d (rim)	[B] (cm^{-3})	Ψ_t (eV)	A** ($Acm^{-2}K^{-2}$)	Ψ_o (eV)	λ_c (pm)	$\Psi_o - \Psi_t$ (eV)
A	0.7	6 x10^{19}	0.218	46	0.217	5.74	-0.001
B	0.9	6x 10^{19}	0.193	72	0.189	6.56	-0.004
C	1.1	6 x10^{19}	0.173	37	0.170	7.3	-0.003
D	1.1	1 x10^{20}	0.112	0.16	0.168	7.38	0.056
E	0.9	2.3 x10^{20}	0.051	0.10	0.088	14,1	0.037